J Therm Anal Calorim (2016) 126:111–119
DOI 10.1007/s10973-016-5499-2

Synthesis, structure, and thermal stability of new scheelite-type $Pb_{1-3x}\square_xPr_{2x}(MoO_4)_{1-3x}(WO_4)_{3x}$ ceramic materials

Magdalena Piątkowska[1] · Elżbieta Tomaszewicz[1]

Received: 15 November 2015 / Accepted: 22 April 2016 / Published online: 7 May 2016

Abstract Monophasic polycrystalline samples of $Pb_{1-3x}\square_xPr_{2x}(MoO_4)_{1-3x}(WO_4)_{3x}$ solid solution with limited homogeneity ($0 < x \le 0.2222$) and cationic vacancies ($\square$) have been prepared by high-temperature annealing of $PbMoO_4/Pr_2(WO_4)_3$ mixtures composed of 40.00 mol% and less of praseodymium tungstate. Initial reactants and obtained ceramic materials were characterized by XRD, simultaneous DTA–TG, IR and UV–Vis–NIR techniques. The X-ray diffraction analysis showed that the monophasic samples crystallize in a tetragonal symmetry, with space group *I4₁/a* (a scheelite-type structure), and $PbMoO_4$ is a matrix of $Pb_{1-3x}\square_xPr_{2x}(MoO_4)_{1-3x}(WO_4)_{3x}$ solid solution. Thermal stability of samples under study strongly depends on concentration of Pr^{3+} ions. The $Pb_{0.9286}\square_{0.0238}Pr_{0.0476}(MoO_4)_{0.9286}(WO_4)_{0.0714}$ solid solution ($x = 0.0238$) shows the highest melting point (1055 °C), and this value is slightly higher than the melting point of $PbMoO_4$ (1040 °C). Lead molybdate and samples of $Pb_{1-3x}\square_xPr_{2x}(MoO_4)_{1-3x}(WO_4)_{3x}$ solid solution are insulators having indirect band gap $E_g > 3$ eV. The observed band gap of monophasic samples shows a nonlinear variation with a change of Pr^{3+} ions concentration in the scheelite framework.

Keywords Scheelite-type structure · Solid solutions · Lead molybdate · Thermal stability

✉ Elżbieta Tomaszewicz
tomela@zut.edu.pl

[1] Department of Inorganic and Analytical Chemistry, West Pomeranian University of Technology, Al. Piastów 42, 71-065 Szczecin, Poland

Introduction

Divalent metal molybdates and tungstates (AMO_4, where M = Ca, Sr, Ba, Ca, Cd, and Pb; M = Mo or W) have wide industrial applications in many fields. They have been used as laser host materials, Raman lasers, optical fibers, humidity sensors, magnetic and photoluminescence materials, and catalysts [1–13]. Among them, lead molybdate and lead tungstate are very attractive materials because of their applications as acousto-optical modulators, deflectors, ion conductors, and solid-state scintillators for a nuclear instrumental application [14–22]. These materials doped with RE^{3+} ions exhibit good photoluminescence, and they are promising as laser hosts [14, 22]. Lead molybdate crystallizes with a scheelite-type tetragonal structure and has a space group (*I4₁/a*), as well as four molecular formulas per unit cell ($Z = 4$) [1, 11, 15, 19, 20, 23, 24]. Its structure is made up of PbO_8 dodecahedra and MoO_4 tetrahedra connected via common vertices (Fig. 1). PbO_8 polyhedra are connected via common edges and form a 3D framework (Fig. 1) [11, 19].

Our earlier studies on a reactivity in a solid state of divalent metal molybdates or tungstates ($CdMoO_4$, $CdWO_4$ and others) with rare-earth compounds (molybdates or tungstates) have been showed an existence of new interesting materials for applications in optoelectronics [25–34]. The scheelite-type ceramic materials, i.e., $Cd_{0.25}RE_{0.50}\square_{0.25}WO_4$ (RE = Pr, Nd, Sm, Eu, and Gd, vacancy is denoted by $\square$), were synthesized via a solid-state reaction of $CdWO_4$ with rare-earth ditungstates $RE_2W_2O_9$ [25–28]. In the scheelite $Cd_{0.25}Gd_{0.50}\square_{0.25}WO_4$ host, where trivalent europium ions occupy only one low symmetry site, a very strong red emission was observed [25]. This Eu^{3+}-doped cadmium and gadolinium tungstate proved to be a new promising polycrystalline red phosphor for

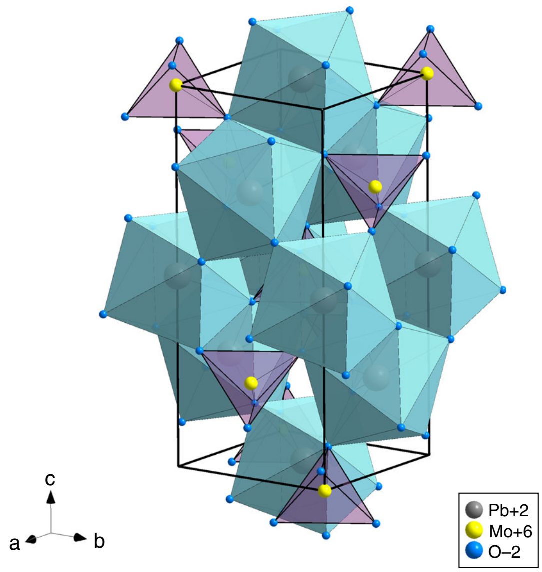

Fig. 1 Structure of $PbMoO_4$ (*cyan*—PbO_8 dodecahedra, *violet*—MoO_4 tetrahedra)

WLEDs [25]. As compared to optical parameters of YAG:Nd, new cadmium and gadolinium tungstate doped with Nd^{3+} ions ($Cd_{0.25}Gd_{0.50}\square_{0.25}WO_4:Nd^{3+}$, the concentration of active ions 5 mol%) showed larger absorption cross section ($2.5 \cdot 10^{-19}$ cm^2 at $\lambda = 805$ nm) and much higher emission at 1064 nm [26]. The broad spectral emission band observed in $Cd_{0.25}Gd_{0.50}\square_{0.25}WO_4:Nd^{3+}$ allows tuning of laser action over the 1030- to 1080-nm range for generation of very short pulses, and therefore, it has applications in pico- or femtosecond lasers [26]. Important group of very good and new candidates for applications in optoelectronics are scheelite-type cadmium and rare-earth metal molybdates $Cd_{1-3x}\square_xRE_{2x}MoO_4$, where RE = Pr–Yb [29–34]. Value of x parameter strongly depends on a radius of trivalent rare-earth ion, and it can reach a maximum value of 0.25 [29–34]. The substitution of divalent cadmium ions by RE^{3+} ones leads to formation of cationic vacancies (□) in $CdMoO_4$ framework [29–34]. The appearance of vacancies results in some disorder of crystal lattice around RE^{3+} ions. This fact is manifested by an emission of broad bands associated with *f–f* transitions in RE^{3+} laser ions (e.g., Nd^{3+} or Yb^{3+}), and this phenomenon could be used for ultrashort laser pulses [30, 31]. Single crystals of some $Cd_{1-3x}\square_xRE_{2x}MoO_4$ (RE = Gd, Dy) solid solutions with different concentrations of RE^{3+} ion have been successfully grown by the Czochralski method [35, 36]. Their structure, dielectric and magnetic properties, and FTIR and Raman spectra were recorded and discussed in detail [35, 36].

The aim of this work is to make a detailed study of new $Pb_{1-3x}\square_xPr_{2x}(MoO_4)_{1-3x}(WO_4)_{3x}$ solid solution that could be used as scintillator material in polycrystalline or single-crystal form. Thus, we present the results on a homogeneity range of the solid solution under study, its structure, and thermal and spectroscopic properties.

Experimental

Sample preparation

Lead molybdate ($PbMoO_4$) and praseodymium tungstate ($Pr_2(WO_4)_3$) were used as the starting materials. Lead molybdate was prepared by heating PbO with MoO_3 (both with the purity 99.95 %, Alfa Aesar) mixed in an equimolar ratio, and in the following thermal conditions: 550 °C (6 h), 600 °C (6 h), 700 °C (6 h), 800 °C (12 h), 900 °C (12 h), and 950 °C (12 h). Praseodymium tungstate was obtained using a solid-state reaction method [37–45] and Pr_6O_{11} with WO_3 (both with the purity 99.95 %, Alfa Aesar) mixed in the 1:9 molar ratio according to the procedure used by us in a synthesis of other rare-earth tungstates, and under thermal conditions reported earlier [25–28, 37–39]. Mixtures of starting reactants with $Pr_2(WO_4)_3$ content changing from 0.50 to 50.00 mol% were homogenized in an agate mortar. Their initial content is presented in Table 1. Next, they were heated in air, in ceramics crucibles, with 12-h annealing stages, and in the temperature range from 900 to 975 °C. After each heating stage, all samples were cooled slowly down to ambient temperature, and for better reactivity, ground in an agate mortar. After a final sintering stage, monophasic samples were examined by XRD, DTA-TG, IR, and UV–Vis–NIR techniques. Additionally, their density was measured.

Methods

Powder X-ray diffraction patterns were collected in the 10–80° 2Θ range with the step 0.013° on a diffractometer Empyrean II (PANalytical) using Cu Kα radiation ($\lambda = 0.15418$ nm). XRD patterns were analyzed by a *HighScore Plus 4.0* software package, and lattice parameters were calculated using the least squares refinement procedure and a POWDER software [47]. Simultaneous DTA and TG measurements were carried out on a TA Instruments thermal analyzer (model SDT 2960) at the heating and cooling rate of 10 °C min^{-1}, in air (the gas flow 110 mL h^{-1}), and using alumina crucibles. The mass of each sample for DTA-TG measurements was ~30 mg. DTA and TG curves were recorded in the temperature range of 20–1100 °C. UV–Vis–NIR diffuse reflectance spectra were recorded at room temperature and in the wavelength range of 190–1000 nm using a JASCO V-670

Table 1 $Pr_2(WO_4)_3$ content in initial $PbMoO_4/Pr_2(WO_4)_3$ mixtures, results of XRD analysis of samples obtained after the last annealing stage (the formula of $Pb_{1-3x}\square_xPr_{2x}(MoO_4)_{1-3x}(WO_4)_{3x}$ was calculated on phase compositions of initial mixtures), calculated lattice constants for an adequate solid solution, calculated as well as experimental values of density, and determined band gap energy

No. of sample	$Pr_2(WO_4)_3$ content/mol%	Formula of solid solution		Lattice constants/nm		Density/g cm^{-3}		Eg/eV
				a	*c*	d_{cal}	d_{exp}	
1	0	$x = 0$	$PbWO_4$ (pure matrix)	0.544105	1.21196	6.80	6.80	3.17
2	0.50	$x = 0.0050$	$Pb_{0.9850}\square_{0.0050}Pr_{0.0100}(MoO_4)_{0.9850}(WO_4)_{0.0150}$	0.543961	1.21162	6.79	6.86	3.14
3	1.00	$x = 0.0098$	$Pb_{0.9706}\square_{0.0098}Pr_{0.0196}(MoO_4)_{0.9706}(WO_4)_{0.0294}$	0.544041	1.21127	6.79	6.87	3.15
4	2.50	$x = 0.0238$	$Pb_{0.9286}\square_{0.0238}Pr_{0.0476}(MoO_4)_{0.9286}(WO_4)_{0.0714}$	0.543885	1.20969	6.78	6.75	3.15
5	5.00	$x = 0.0455$	$Pb_{0.8635}\square_{0.0455}Pr_{0.0910}(MoO_4)_{0.8635}(WO_4)_{0.1365}$	0.543216	1.20765	6.78	6.74	3.16
6	10.00	$x = 0.0839$	$Pb_{0.7483}\square_{0.0839}Pr_{0.1678}(MoO_4)_{0.7483}(WO_4)_{0.2517}$	0.542529	1.20251	6.77	6.74	3.18
7	20.00	$x = 0.1430$	$Pb_{0.5710}\square_{0.1430}Pr_{0.2860}(MoO_4)_{0.5710}(WO_4)_{0.4290}$	0.541150	1.19959	6.73	6.76	3.20
8	25.00	$x = 0.1667$	$Pb_{0.4999}\square_{0.1667}Pr_{0.3334}(MoO_4)_{0.4999}(WO_4)_{0.5001}$	0.539606	1.19606	6.76	6.79	3.21
9	33.33	$x = 0.2000$	$Pb_{0.4000}\square_{0.2000}Pr_{0.4000}(MoO_4)_{0.4000}(WO_4)_{0.6000}$	0.538082	1.19256	6.77	6.74	3.22
10	40.00	$x = 0.2222$	$Pb_{0.3334}\square_{0.2222}Pr_{0.4444}(MoO_4)_{0.3334}(WO_4)_{0.6666}$	0.537727	1.19076	6.76	6.75	3.21
11	50.00	$Pb_{0.3334}\square_{0.2222}Pr_{0.4444}(MoO_4)_{0.3334}(WO_4)_{0.6666}$, $Pr_2(WO_4)_3$		0.537727	1.19076	Not determined		

spectrophotometer equipped with an integrating sphere. The reflectance measurements were carried out using scan step 0.5 nm and scan speed 400 nm/min. IR spectra of samples were collected in the 1500–200 cm^{-1} spectral range on a Specord M-80 spectrometer (Carl Zeiss Jena) using pellets with KBr. The density of samples was measured on a Quantachrome Instruments Ultrapycnometer (model Ultrapyc 1200 e) using nitrogen (99.99 %) as a pycnometric gas. The measurements were carried out in five repetitions using ~4 g of each sample for the test. The error determine a density was estimated as ±0.01 g cm^{-3}.

Results and discussion

XRD and IR studies

The X-ray powder diffraction patterns of initial reactants and all samples under study were recorded and analyzed. Figure 2 shows experimental XRD patterns of $PbMoO_4$ and products obtained after the final sintering stage of some $PbMoO_4/Pr_2(WO_4)_3$ mixtures. It was observed that when the initial content of praseodymium tungstate was 40.00 mol% and less, the XRD patterns consisted of diffraction lines that could be attributed to a scheelite-type lattice. No additional peaks of other phases, e.g., initial reactants, have been observed. Additionally, all observed diffraction peaks shift toward higher 2θ angle with an increase in $Pr_2(WO_4)_3$ content in initial mixtures. Very sharp and strong peaks clearly confirm good crystallinity of the as-prepared samples. All diffractions lines observed in the XRD patterns of single-phase materials were successfully indexed with a tetragonal symmetry and space group $I4_1/a$. This fact has indicated a formation of a new solid

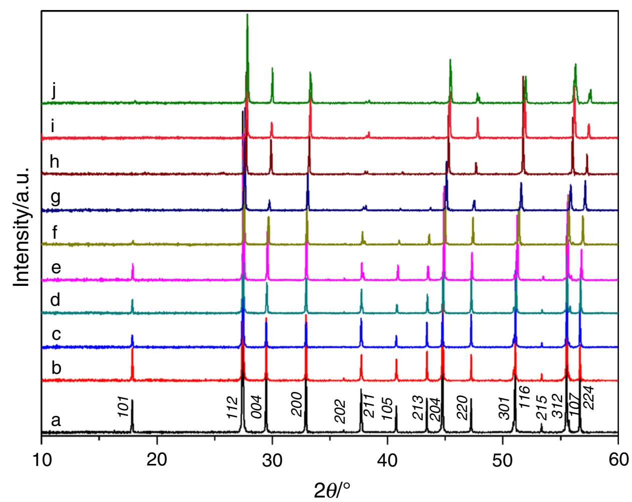

Fig. 2 Powder XRD patterns of $PbMoO_4$ (**a**), $Pb_{1-3x}\square_xPr_{2x}(MoO_4)_{1-3x}(WO_4)_{3x}$ for: $x = 0.0050$ (**b**); $x = 0.0098$ (**c**); $x = 0.0238$ (**d**); $x = 0.0455$ (**e**); $x = 0.0839$ (**f**); $x = 0.1430$ (**g**); $x = 0.1667$ (**h**); $x = 0.2000$ (**i**); $x = 0.2222$ (**j**)

solution and its synthesis can be described by the following equation:

$$(1-3x)\ PbMoO_{4(s)} + xPr_2(WO_4)_{3(s)} = Pb_{1-3x}\square_xPr_{2x}(MoO_4)_{1-3x}(WO_4)_{3x(s)} \quad (1)$$

A location of this solution is marked in the tetrahedron of $PbO–WO_3–Pr_2O_3–MoO_3$ system (Fig. 3). The lattice constants calculated by cell refinement fitting on the basis of XRD data for an adequate $Pb_{1-3x}\square_xPr_{2x}(MoO_4)_{1-3x}(WO_4)_{3x}$ solid solution identified in monophasic samples (Nos. 2–10), as well as experimental and calculated values of density are presented in Table 1. The cell parameters gradually decrease with an increase in value of x parameter only up to 0.2222 suggesting the solid solution limit has been achieved. Both, unit cell parameters and volume calculated for single-phase samples fulfill the Vegard law, i.e., are nearly linear function of x (Fig. 4). The diffraction pattern of a sample comprising initially 50.00 mol% of $Pr_2(WO_4)_3$ consisted of diffraction lines due to $Pb_{0.3334}\square_{0.2222}Pr_{0.4444}(MoO_4)_{0.3334}(WO_4)_{0.6666}$ (the saturated solid solution), and additionally, the peaks corresponding to praseodymium tungstate have appeared. The above observations indicate that the solubility limit of $Pr_2(WO_4)_3$ in a scheelite-type framework of $PbMoO_4$ is not higher than 40.00 mol% and $Pb_{1-3x}\square_xPr_{2x}(MoO_4)_{1-3x}(WO_4)_{3x}$ solid solution exists for $0 < x \leq 0.2222$. Moreover, the results have indicated that Pr^{3+} (CN (coordination number) = 8, ionic radius −112.6 pm [46]) and W^{6+} (CN = 4, 42 pm [46]) ions were introduced to $PbMoO_4$ matrix instead of Pb^{2+} (CN = 8, 129 pm [46]) and Mo^{6+} (CN = 4, 41 pm [46]) ions, respectively. Compensation of excess positive charge resulting from substitution of divalent ions by trivalent ones is accomplished by an appearance of cationic vacancies denoted as $\square$.

Figure 5 shows IR spectra recorded for polycrystalline samples of $PbMoO_4$ and $Pb_{1-3x}\square_xPr_{2x}(MoO_4)_{1-3x}(WO_4)_{3x}$ with different concentration of Pr^{3+} ions. For solid molybdates with a scheelite-type structure, the frequencies active in IR are observed in the wave number ranges 900–700 cm^{-1} (the stretching multiples ν_1 and ν_3) and 450–250 cm^{-1} (the bending modes ν_2 and ν_4) [33, 34, 48, 49]. Very narrow absorption bands can be observed in the IR spectrum of $PbMoO_4$ (pure matrix). The first group of bands sequentially recorded at 853, 816, and 768 cm^{-1} can be assigned to the stretching modes of Mo–O bonds in MoO_4 tetrahedra [33, 34, 48, 49]. On the other hand, the absorption bands with their maxima at 380 and 296 cm^{-1} can be related to the bending modes of Mo–O bonds in MoO_4 tetrahedra [33, 34, 48, 49]. The experimental results for pure lead molybdate confirm the presence of only regular MoO_4 tetrahedra occupying sites with the S_4 symmetry in scheelite-type framework. In the case of IR spectra of the samples of solid solution, an additional absorption band, apart to those ones

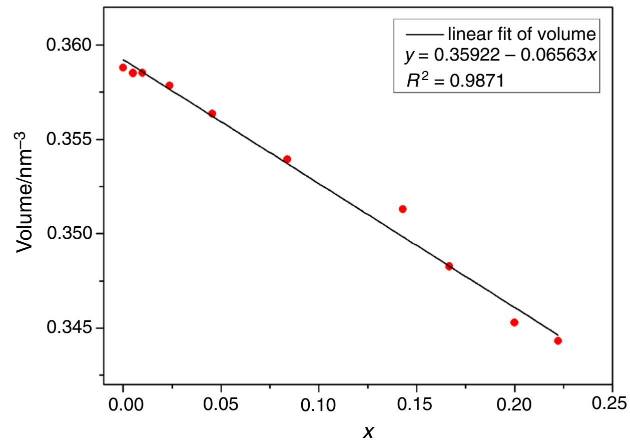

Fig. 4 Linear fit of cell volume of $Pb_{1-3x}\square_xPr_{2x}(MoO_4)_{1-3x}(WO_4)_{3x}$ solid solution versus x parameter

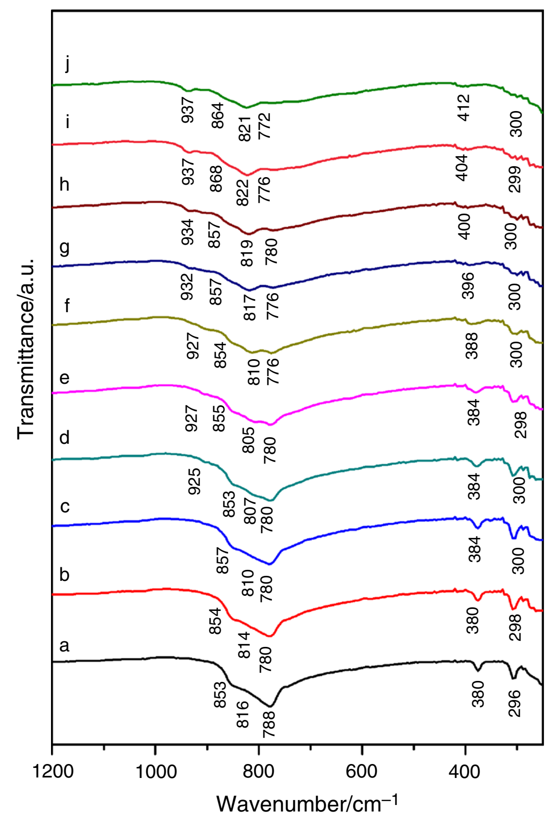

Fig. 5 IR spectra of $PbMoO_4$ (**a**), $Pb_{1-3x}\square_xPr_{2x}(MoO_4)_{1-3x}(WO_4)_{3x}$ for: $x = 0.0050$ (**b**); $x = 0.0098$ (**c**); $x = 0.0238$ (**d**); $x = 0.0455$ (**e**); $x = 0.0839$ (**f**); $x = 0.1430$ (**g**); $x = 0.1667$ (**h**); $x = 0.2000$ (**i**); $x = 0.2222$ (**j**)

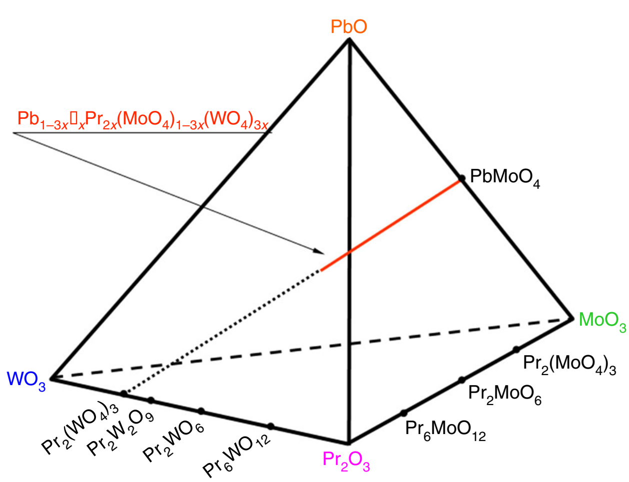

Fig. 3 Tetrahedron of the $PbO–WO_3–Pr_2O_3–MoO_3$ system with a location of $Pb_{1-3x}\square_xPr_{2x}(MoO_4)_{1-3x}(WO_4)_{3x}$ solid solution

recorded for $PbMoO_4$, was observed (Fig. 5). This band is clearly visible in the IR spectra of $Pb_{1-3x}\square_xPr_{2x}(MoO_4)_{1-3x}(WO_4)_{3x}$ for $x \geq 0.0238$ (at 925 cm^{-1} for $x = 0.0238$), and it moves toward higher wavenumbers up to 937 cm^{-1} (the saturated solid solution). Additionally, the intensity of this band significantly increases with increasing of praseodymium ions content in samples under study. Moreover, the absorption bands due to the stretching as well as bending modes of Mo–O bonds in MoO_4 tetrahedra observed also in the IR spectra of $PbMoO_4$ clearly move toward higher wave numbers when a concentration of praseodymium ions increased in doped samples. This fact suggests the presence of WO_4 tetrahedra in crystal lattice of $Pb_{1-3x}\square_xPr_{2x}(MoO_4)_{1-3x}(WO_4)_{3x}$ [48, 49]. The appearance of additional absorption band and a change in its position suggests the presence of other types of molybdenum and tungsten polyhedra, i.e., distorted MoO_4 as well as WO_4 tetrahedra with cationic vacancy near one or two corners of MoO_4 and WO_4. The same phenomenon has been observed in the case of a similar solid solution with gadolinium ions ($Cd_{1-3x}\square_xGd_{2x}MoO_4$) [33, 34]. Gradual increase in the intensity of the additional IR band (at ~930 cm^{-1}) and simultaneous reduction in the intensity of the bands observed at 853, 816, 768, 380, and 296 cm^{-1} indicate the increasing number of deformed MoO_4 and WO_4 tetrahedra in comparison with a number of regular ones. It seems to be evident because with increase in concentration of Pr^{3+} ions the number of vacancies generated in the crystal structure of $Pb_{1-3x}\square_xPr_{2x}(MoO_4)_{1-3x}(WO_4)_{3x}$ solid solution is increased.

DTA-TG studies

Appropriate DTA-TG studies of obtained ceramic materials were preceded by similar studies for $PbMoO_4$ and $Pr_2(WO_4)_3$. Figure 6 shows DTA curves of $PbMoO_4$ (TG curve is not presented here) recorded during heating and cooling runs. The endothermic effect started at 1040 °C is due to congruent melting of lead molybdate. The crystallization process from a melt starts at a little higher temperature, i.e., 1053 °C. These results are similar to those ones obtained by Senguttuvan et al. and by Zeng [21, 50]. Lead molybdate does not show polymorphism. Two endothermic effects were observed on the DTA curve recorded during controlled heating of $Pr_2(WO_4)_3$ (Fig. 7, TG curve is not presented). The first one started at 1037 °C is connected with a phase transformation of a monoclinic α-$Pr_2(WO_4)_3$ (space group *C2/c*) to a high-temperature polymorph (β) with a orthorhombic symmetry (space group *Pnca*, a structure of $Sc_2(MoO_4)_3$-type) [51, 52]. A similar polymorphic change is observed in other rare-earth metal tungstates, e.g., for $Gd_2(WO_4)_3$ [38]. Praseodymium tungstate melts congruently in air at 1112 °C (the second endothermic effect on DTA curve of this compound recorded during controlled heating). The crystallization process from a melt and the phase transition of β- to α-polymorph start at 1107 and 903 °C, respectively (Fig. 7). Figure 8 shows DTA curves of some samples of $Pb_{1-3x}\square_xPr_{2x}(MoO_4)_{1-3x}(WO_4)_{3x}$ solid solution (Nos. 2–10). On each DTA curve only one endothermic effect (symmetrical or asymmetrical) was recorded. This effect was caused by melting of each sample under study. When a concentration of Pr^{3+} ions in $PbMoO_4$ matrix increased up to $x = 0.0238$ (up to 2.50 mol% of praseodymium tungstate in initial $PbMoO_4/Pr_2(WO_4)_3$ mixtures), the onset of endothermic peak increased up to 1055 °C. The endothermic effects recorded on DTA curves of monophasic samples for $x \geq 0.0455$ are clearly asymmetric with a visible inflection observed at a temperature slightly lower than a minimum temperature of each effect. This inflection can suggest a simultaneous presence of two endothermic peaks with slightly different onsets. In a case of $Pb_{1-3x}\square_xPr_{2x}(MoO_4)_{1-3x}(WO_4)_{3x}$ samples for $x \geq 0.0455$, the onset of observed peaks decreased from 1048 up to 1025 °C (for the saturated solid solution). In the whole homogeneity range melting point of $Pb_{1-3x}\square_xPr_{2x}(MoO_4)_{1-3x}(WO_4)_{3x}$ samples shows nonlinear dependence on x parameter.

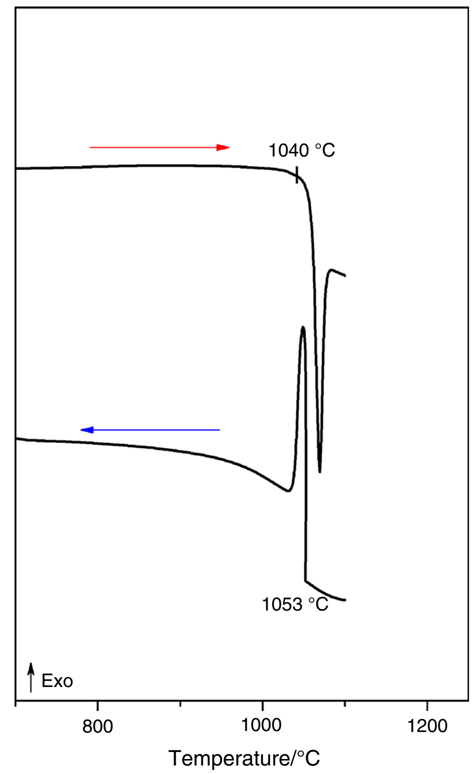

Fig. 6 DTA curves of $PbMoO_4$ recorded during controlled heating and cooling runs

UV–Vis–NIR spectra and band gap determination

The band gap energy, E_g, is a very important attribute of semiconductors because it determines their applications, e.g., in optoelectronics. Optical absorption studies are used

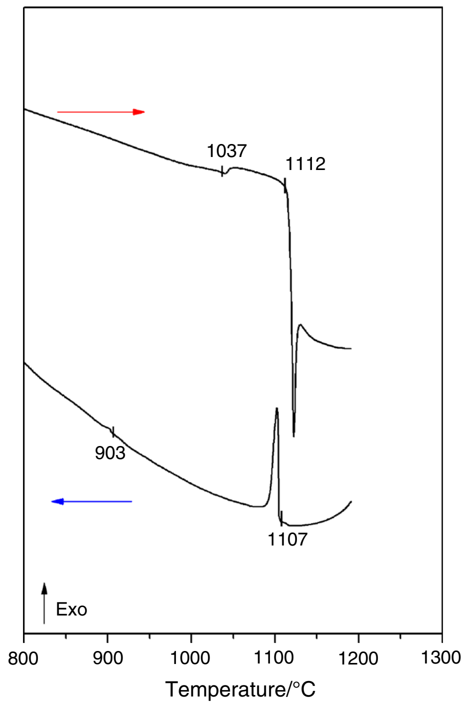

Fig. 7 DTA curves of $Pr_2(WO_4)_3$ recorded during controlled heating and cooling runs

to characterize the electronic properties of materials, through the determination of such parameters as band gap and excited state lifetime. The band gap for bulk $PbMoO_4$ and samples of $Pb_{1-3x}\square_xPr_{2x}(MoO_4)_{1-3x}(WO_4)_{3x}$ solid solution was determined from their diffuse reflectance spectra showed in Fig. 9. The reflectance data were converted into absorption ones using the Kubelka–Munk function according to the following Eq. [53]:

$$F(R) = (1 - R)^2/2R \tag{2}$$

where R is reflectance and $F(R)$ is the Kubelka–Munk transformation. It is known that the band gap E_g and absorption coefficient α are related as in the following Eq. [53]:

$$F(R) \cdot hv = \alpha \cdot hv = A(hv - E_g)^n \tag{3}$$

where A is a constant characteristic for material under study, h is the Plank constant, v is light frequency, and n is a constant associated with the different types of electronic transitions (n = 1/2, 2, 3/2, or 3) depending upon an nature of electronic transitions responsible for an absorption [54]. The Tauc optical gap for $PbMoO_4$ and monophasic samples of solid solution was determined through an extrapolation of the linear trend observed in the spectral dependence of $(\alpha \cdot hv)^{1/n}$, i.e., $[F(R) \cdot hv]^{1/n}$ over a limited range of photon energies hv. The values of band gap energy for $n = 2$, i.e., for indirect allowed transition of an electron from a valance to a conduction band are showed in Table 1. The E_g value for $PbMoO_4$ was found to be 3.17 eV, and this value is very close to those ones reported

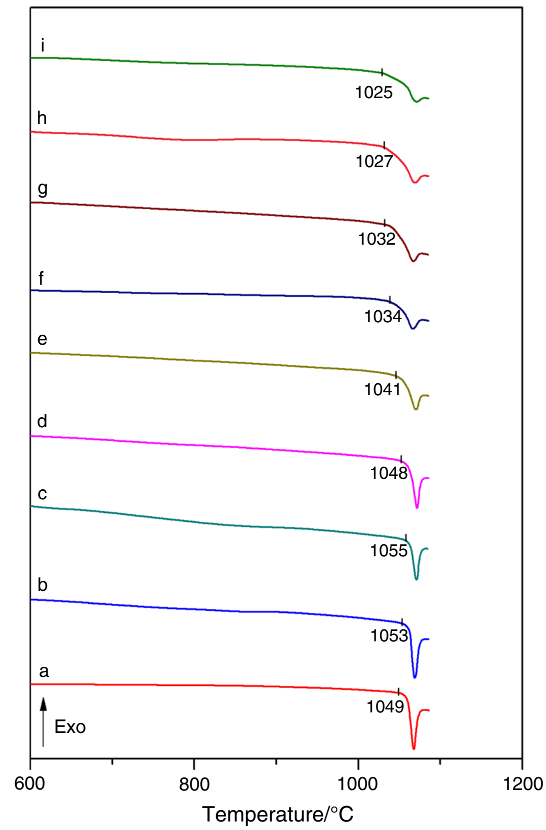

Fig. 8 DTA curves of $Pb_{1-3x}\square_xPr_{2x}(MoO_4)_{1-3x}(WO_4)_{3x}$ for: $x = 0.0050$ (**a**); $x = 0.0098$ (**b**); $x = 0.0238$ (**c**); $x = 0.0455$ (**d**); $x = 0.0839$ (**e**); $x = 0.1430$ (**f**); $x = 0.1667$ (**g**); $x = 0.2000$ (**h**); $x = 0.2222$ (**i**)

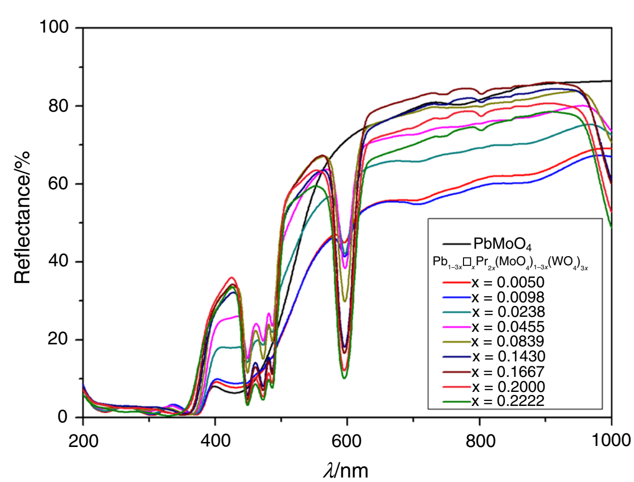

Fig. 9 UV-vis–NIR diffuse reflectance spectra of $PbMoO_4$ and $Pb_{1-3x}\square_xPr_{2x}(MoO_4)_{1-3x}(WO_4)_{3x}$ for different values of x parameter

earlier, i.e., 3.14–3.19 eV [22], 3.20 eV [23], and 3.30 eV [1]. The observed band gap of $Pb_{1-3x}\square_xPr_{2x}(MoO_4)_{1-3x}(WO_4)_{3x}$ samples increases from 3.14 eV ($x = 0.0050$) up to 3.22 eV ($x = 0.2000$). The E_g value of saturated solid solution, i.e., $Pb_{0.3334}\square_{0.2222}Pr_{0.4444}(MoO_4)_{0.3334}(WO_4)_{0.6666}$ ($x = 0.2222$)

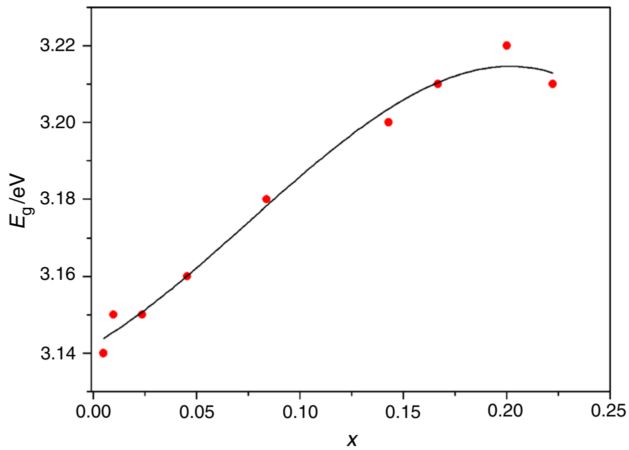

Fig. 10 Dependence of band gap energy (E_g) on x parameter

is a slightly lower and equals 3.21 eV. It was also shown a nonlinear (parabolic) variation in the band gap with x parameter (Fig. 10). Similar dependence of E_g (nonlinear) on x parameter was observed for scheelite $Ca_{1-x}Sr_xMoO_4$ solid solution [55].

Conclusions

Polycrystalline samples of new $Pb_{1-3x}\square_xPr_{2x}(MoO_4)_{1-3x}(WO_4)_{3x}$ solid solution, where □ are cationic vacancies, have been successfully synthesized by a solid-state reaction at the temperatures ranging from 900 to 975 °C. As the starting materials for synthesis, $PbMoO_4$ and $Pr_2(WO_4)_3$ were used. The homogeneity range of solid solution under study is $0 < x \leq 0.2222$, i.e., the maximum content of praseodymium tungstate in initial $PbMoO_4/Pr_2(WO_4)_3$ equals 40.00 mol%. All monophasic samples crystallize in a tetragonal body-centered scheelite-type structure. Samples of $Pb_{1-3x}\square_xPr_{2x}(MoO_4)_{1-3x}(WO_4)_{3x}$ solid solution do not show polymorphism, and their melting point strongly depends on a value of x parameter. The highest melting point, i.e., 1055 °C is for a solid solution with $x = 0.0238$, and this temperature is slightly higher than a melting point of pure matrix ($PbMoO_4$, 1040 °C). IR spectra showed a presence of MoO_4 and WO_4 tetrahedra in the scheelite structure of new phases. Additionally, in comparison to regular MoO_4/WO_4 tetrahedra occupying sites with the S_4 symmetry in a scheelite-type framework, a some deformation of MoO_4 and WO_4 tetrahedra in structure of $Pb_{1-3x}\square_xPr_{2x}(MoO_4)_{1-3x}(WO_4)_{3x}$ is observed. Both, pure matrix ($PbMoO_4$) and samples of $Pb_{1-3x}\square_xPr_{2x}(MoO_4)_{1-3x}(WO_4)_{3x}$ solid solution are insulators with indirect band gap $E_g > 3$ eV. The nonlinear dependence of E_g on a value of x parameter is also observed.

References

1. Bi JH, Wu L, Zhang YF, Li ZhH, Li JQ, Fu ZhX. Solvothermal preparation, electronic structure and photocatalytic properties of $PbMoO_4$ and $SrMoO_4$. Appl Catal B. 2009;91:135–43.
2. Babin V, Bohacek P, Bender E, Krasnikov A, Mihokova E, Nikl M, Senguttuvan N, Stolovits A, Usuki Y, Zazubovich S. Decay kinetics of the green emission in tungstates and molybdates. Radiat Meas. 2004;38:533–7.
3. Wang J, Li X, Luo L, Zhang S, Lu R. Core–shell $BaMoO_4$@SiO_2 nanospheres: preparation, characterization, and optical properties. Ceram Int. 2013;39:9293–8.
4. Choi GK, Kim JR, Yoon SH, Hong KS. Microwave dielectric properties of scheelite (A = Ca, Sr, Ba) and wolframite (A = Mg, Zn, Mn) $AMoO_4$ compounds. J Eur Ceram Soc. 2007;27:3063–7.
5. Azevedo Marques AP, de Melo DMA, Longo E, Paskocimas CA, Pizani PS, Leite ER. Photoluminescence properties of $BaMoO_4$ amorphous thin films. J Solid State Chem. 2005;178:2346–53.
6. Sczancoski JC, Cavalcante LS, Joya MR, Varela JA, Pizani PS, Longo E. $SrMoO_4$ powders processed in microwave-hydrothermal: synthesis, characterization and optical properties. Chem Eng J. 2008;140:632–7.
7. Kim MJ, Huh YD. Synthesis and optical properties of $CaMoO_4:Eu^{3+}$, Na^+ nanophosphors and a transparent $CaMoO_4:Eu^{3+}$, Na^+ suspension. Opt Mater. 2012;35:263–7.
8. Boulon G. Fifty years of advances in solid-state laser materials. Opt Mater. 2012;34:499–512.
9. Shivakumara C, Saraf R. Eu^{3+}-activated $SrMoO_4$ phosphors for white LEDs applications: synthesis and structural characterization. Opt Mater. 2015;42:178–86.
10. Hernández-Uresti DB, Martínez-de la Cruz A, Aguilar-Garib JA. Photocatalytic activity of $PbMoO_4$ molybdate synthesized by microwave method. Catal Today. 2013;212:70–4.
11. Sczancoski JC, Bomio MDR, Cavalcante LS, Joya MR, Pizani PS, Ravela JA, Longo E, Siu Li M, Andrés JA. Morphology and blue photoluminescence emission of $PbMoO_4$ processed in conventional hydrotermal. J Phys Chem C. 2009;113:5812–22.
12. Doroshenko ME, Basiev TT, Vassiliev SV, Ivleva LI, Komar VK, Kosmyna MB, Jelínkova H, Šulc J. Comparative study of the lasing properties of self-Raman capable Nd^{3+} doped tungstates and molybdates under diode pumping. Opt Mater. 2007;30:54–7.
13. Gyawali G, Adhikari R, Joshi B, Ho Kim T, Rodríguez-Gonzáles V, Wohn Lee S. Sonochemical synthesis of solar-light-driven Ag°-$PbMoO_4$ photocatalyst. J Hazard Mater. 2013;263:45–51.
14. Aghamalyan NR, Demirkhanyan GG, Hovsepyan RK, Kostanyan RB, Zargaryan DG. Room-temperature near infrared emission and green up-conversion in $PbMoO_4:Er^{3+}$ crystals. Opt Mater. 2010;32:1046–9.
15. Xing G-J, Liu R, Zhao C, Li Y-L, Wang Y, Wu G-M. Photoluminescence and photocatalytic properties of uniform $PbMoO_4$ polyhedral crystals synthesized by microemulsion-based solvothermal method. Ceram Int. 2011;37:2951–6.

16. Nedilko S, Chornii V, Hizhnyi Y, Trubitsyn M, Volnyanskaya I. Luminescence spectroscopy and electronic structure of the $PbMoO_4$ and Pb_2MoO_5 single crystals. Opt Mater. 2014;36:1754–9.
17. Danevich FA, Grinyov BV, Henry S, Kosmyna MB, Kraus H, Krutyak N, Kudovbenko VM, Mikhailik VB, Nagornaya LL, Nazarenko BP, Nikolaiko AS, Polischuk OG, Puzikov VM, Shekhovtsov AN, Tretyak VI, Vostretsov YY. Feasibility study of $PbWO_4$ and $PbMoO_4$ crystal scintillators for cryogenic rare events experiments. Nucl Instr Meth Phys Res A. 2010;622:608–13.
18. Phuruangrat A, Thongtem T, Thongtem S. Analysis of lead molybdate and lead tungstate synthesized by a sonochemical method. Curr Appl Phys. 2010;10:342–5.
19. Bomio MRD, Cavalcante LS, Almeida MAP, Tranquilin RL, Batista NC, Pizani PS, Andrés J, Siu Li M, Longo E. Structural refinement, growth mechanism, infrared/Raman spectroscopies and photoluminescence properties of $PbMoO_4$ crystals. Polyhedron. 2013;50:532–45.
20. Phuruangrat A, Thongtem T, Thongtem S. Synthesis of lead molybdate and lead tungstate via microwave irradiation method. J Cryst Growth. 2009;311:4076–81.
21. Senguttuvan N, Moorthy Babu S, Subramanian C. Synthesis, crystal growth and mechanical properties of lead molybdate. Mat Sci Eng B. 1997;47:269–73.
22. Gorobets YN, Kosmyna MB, Luchechko AP, Nazarenko BP, Puzikov VM, Shekhovtsov AN, Sugak DY. Crystal growth of $PbWO_4:Nd^{3+}$ and $PbMoO_4:Nd^{3+}$ crystals and their characterization by means optical and dielectric relaxation spectroscopy. J Cryst Growth. 2011;318:687–90.
23. Kwolek P, Tokarski T, Łokcik T, Szaciłowski K. Novel, microwave assisted route of synthesis of binary oxide semiconducting phases–$PbMoO_4$ and $PbWO_4$. Arch Metall Mater. 2013;58:217–22.
24. Chen J, Zhang Q, Liu T, Shao Z. First-principles study of color centers in $PbMoO_4$ crystals. Phys B. 2008;403:555–8.
25. Guzik M, Tomaszewicz E, Kaczmarek SM, Cybińska J, Fuks H. Spectroscopic investigations of $Cd_{0.25}Gd_{0.50}\square_{0.25}WO_4:Eu^{3+}$: a new promising red phosphor. J Non-Cryst Solids. 2010;356:1902–7.
26. Guzik M, Tomaszewicz E, Guyot Y, Legendziewicz J, Boulon G. Structural and spectroscopic characterizations of two promising Nd-doped monoclinic or tetragonal laser tungstates. J Mater Chem. 2012;22:14896–906.
27. Tomaszewicz E, Kaczmarek SM, Fuks H. New cadmium and rare-earth metal tungstates with the sheelite type structure. J Rare Earths. 2009;27:569–73.
28. Tomaszewicz E, Fuks H, Typek J. Synthesis, thermal stability and magnetic properties of novel cadmium and praseodymium tungstate $Cd_{0.25}Pr_{0.50}\square_{0.25}WO_4$ and its solid solutions. Thermochim Acta. 2013;568:95–103.
29. Tomaszewicz E, Filipek E, Fuks H, Typek J. Thermal and magnetic properties of new scheelite type $Cd_{1-3x}\square_xGd_{2x}MoO_4$ ceramic materials. J Eur Ceram Soc. 2014;34:1511–22.
30. Guzik M, Tomaszewicz E, Guyot Y, Legendziewicz J, Boulon G. Structural and spectroscopic characterizations of new vacancied $Cd_{1-3x}Nd_{2x}\square_xMoO_4$ scheelite-type molybdates as potential optical materials. J Mater Chem C. 2015;3:4057–69.
31. Guzik M, Tomaszewicz E, Guyot Y, Legendziewicz J, Boulon J. Spectroscopic properties, concentration quenching and Yb^{3+} site occupations in a vacancied scheelite-type molybdates. J Lumin. 2016;169:755–64.
32. Guzik M, Tomaszewicz E, Guyot Y, Legendziewicz J, Boulon G. Eu^{3+} luminescence from different sites in scheelite-type cadmium molybdate red phosphor with vacancies. J Mater Chem C. 2015;3:8582–94.
33. Godlewska P, Tomaszewicz E, Macalik L, Hanuza J, Ptak M, Tomaszewski P, Mączka M, Ropuszyńska-Robak P. Correlation between the structural and spectroscopic parameters for $Cd_{1-3x}Gd_{2x}\square_xMoO_4$ solid solutions where □ denotes cationic vacancies. Mater Chem Phys. 2013;139:890–6.
34. Godlewska P, Tomaszewicz E, Macalik L, Hanuza J, Ptak M, Tomaszewski PE, Ropuszyńska-Robak P. Structure and vibrational properties of scheelite type $Cd_{0.25}RE_{0.5}\square_{0.25}MoO_4$ solid solutions where □ is the cationic vacancy and RE = Pr, Nd, Sm–Dy. J Mol Struct. 2013;1037:332–7.
35. Groń T, Tomaszewicz E, Berkowski M, Duda H, Kukuła Z, Pawlus S, Mydlarz T, Ostafin T, Kusz J. Dielectric and magnetic properties of $CdMoO_4:Gd^{3+}$ single crystal. J Alloys Compd. 2014;593:230–4.
36. Macalik L, Tomaszewicz E, Ptak M, Hanuza J, Berkowski M, Mączka M, Ropuszyńska-Robak P. Polarized Raman and IR spectra of oriented $Cd_{0.9577}Gd_{0.0282}\square_{0.0141}MoO_4$ and $Cd_{0.9346}Dy_{0.0436}\square_{0.0218}MoO_4$ single crystals where □ denotes the cationic vacancies. Spectrochim Acta A. 2015;148:255–9.
37. Kukuła Z, Tomaszewicz E, Mazur S, Groń T, Pawlus S, Duda H, Mydlarz T. Electrical and magnetic properties of $CdRE_2W_2O_{10}$ tungstates (RE = Y, Nd, Sm, Gd-Er). J Phys Chem Solids. 2013;74:86–93.
38. Tomaszewicz E, Fuks H, Typek J, Sawicki B, Oboz M, Groń T, Mydlarz T. Preparation, thermal stability and magnetic properties of new $AgY_{1-x}Gd_x(WO_4)_2$ ceramic materials. Ceram Int. 2015; 41:5734–48.
39. Sawicki B, Groń T, Tomaszewicz E, Duda H, Górny K. Some optical and transport properties of a new subclass of ceramic tungstates and molybdates. Ceram Int. 2015;41:13080–9.
40. Šulcová P, Stránská L, Proklešková E. Study of Bi_2O_3 doped by rare-earth element. J Therm Anal Calorim. 2013;113:1203–8.
41. Öztürk E, Kalaycioglu Ozpozan N. Mn^{4+}-, $Tb^{3+,4+}$-, and Er^{3+}-activated red phosphors in the $MgAl_2Si_2O_8$ system. J Therm Anal Calorim. 2014;115:573–7.
42. Öztürk E, Kalaycioglu Ozpozan N, Dayan S. Novel red-emitting phosphors, $(Mg_{(1-x-y)}Mn_xDy_y)Al_2Si_2O_8$ and $(Mg_{(1-x-y)}Mn_xTm_y)Al_2Si_2O_8$. J Therm Anal Calorim. 2014;117:573–8.
43. Öztürk E, Karacaoglu E. Luminescence properties of M_2TiO_4:-Eu^{3+}, Li^+, (M:Mg, Ca) and $MgAl_2O_4:RE^{3+}$ ($RE^{3+}:Ho^{3+}$, Sm^{3+}, and Yb^{3+}). J Therm Anal Calorim. 2015;119:1063–71.
44. Öztürk E, Karacaoglu E. Investigation of phase formation dependency of photoluminescence properties of Eu^{3+} in $Mg_4Al_2O_7:Eu^{3+}$, Dy^{3+}, and $Ca_4Al_2O_7:Eu^{3+}$, Dy^{3+} red-emitting phosphors. J Therm Anal Calorim. 2015;120:1139–43.
45. Opravil T, Ptáček P, Šoucal F, Bartoníčková E, Wasserbauer J. Solid-state synthesis of SrY_2O_4 and $SrSm_2O_4$. J Therm Anal Calorim. 2016;123:181–94.
46. Shannon RD. Revised effective ionic radii and systematic studies of interatomic distances in halides and chalcogenides. Acta Crystallogr A. 1976;32(5):751–67.
47. Taupin D. A powder-diagram authomatic-indexing routine. J Appl Crystallogr. 1973;6:380–5.
48. Tsaryuk VI, Zolin VF. Vibration and vibronic spectra of lanthanide compounds with different types of coordination polyhedra of tungsten and molybdenum. Spectrochim Acta A. 2001;57:355–9.
49. Hanuza J, Mączka M, van der Maas JH. Polarized IR and Raman spectra of tetragonal $NaBi(WO_4)_2$, $NaBi(MoO_4)_2$ and $LiBi(MoO_4)_2$ single crystals with scheelite structure. J Mol Struct. 1995;348:349–52.
50. Zeng HC. Correlation of $PbMoO_4$ crystal imperfections to Czochralski growth process. J Cryst Growth. 1997;171:136–45.
51. Brixner LH, Sleight AW. Crystal growth and precision lattice constants of some $Ln_2(WO_4)_3$-type rare earth tungstates. Mat Res Bull. 1973;8:1269–74.

52. Nassau K, Levinstein HJ, Loiacono GM. A comprehensive study of trivalent tungstates and molybdates of the type $L_2(MO_4)_3$. J Phys Chem Solids. 1965;26:1805–16.
53. Kubelka P, Munk F. Ein Beitrag zur Optic der Farbanstriche. Z Tech Phys. 1931;12:593–601.
54. Tauc J, Grigorovici R, Vancu A. Optical properties and electronic structures of amorphous germanium. Phys Status Solid. 1966;15:627–37.
55. Ramarao SD, Roopas Kiran S, Murthy VRK. Structural, lattice vibrational, optical and micowave dielectric studies on $Ca_{1-x}Sr_{x}$-MoO_4 ceramics with scheelite structure. Mat Res Bull. 2014;56:71–9.